ACS OMEGA

Open Access

http://pubs.acs.org/journal/acsodf

Article

In situ Growth of Zeolite Imidazole Frameworks (ZIF-67) on Carbon Cloth for the Application of Oxygen Reduction Reactions and Microbial Fuel Cells

Mohammed Al Murisi, Sameer Al-Asheh,* Mohammad Ali Abdelkareem, Ahmad Aidan, Khaled Elsaid, and Abdul Ghani Olabi

Cite This: *ACS Omega* 2023, 8, 44514−44522

Read Online

ACCESS | Metrics & More | Article Recommendations | Supporting Information

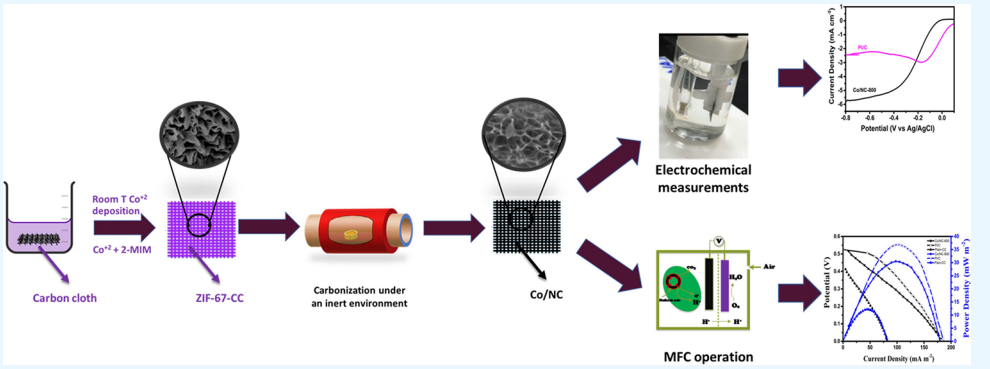

ABSTRACT: Developing high surface area catalysts is an effective strategy to enhance the oxygen reduction reaction (ORR) in the application of microbial fuel cells (MFCs). This can be achieved by developing a catalyst based on metal−organic frameworks (MOFs) because they offer a porous active site for ORR. In this work, a novel in situ growth of 2D shell nanowires of ZIF-67 as a template for N-doped carbon (Co/NC) via a carbonization route was developed to enhance the ORR performance. The effects of different reaction times and different annealing temperatures were studied for a better ORR activity. The growth of the MOF template on the carbon cloth was confirmed using scanning electron microscopy, field emission scanning electron microscopy, transmission electron microscopy, X-ray diffraction, X-ray photoelectron spectroscopy, and Fourier transform infrared. The Co/NC-800 exhibited an enhancement in the ORR activity as evidenced by an onset potential and half-wave potential of 0.0 vs V Ag/AgCl and −0.1 vs V Ag/AgCl, respectively, with a limited current density exceeding the commercial Pt/C. Operating Co/NC-800 on MFC revealed a maximum power density of 30 ± 2.5 mW/m^2, a maximum current density of 180 ± 2.5 mA/m^2.

1. INTRODUCTION

In recent years, global demand for energy and its environmental impact have become controversial issues for the whole world due to continuous population growth and due to environmental issues associated with global warming and air pollution including CO_2, SO_2, and NO_x emissions. The Intergovernmental Panel on Climate Change reported that the impact of greenhouse gas emissions from burning fossil fuels is expected to likely increase the temperature by 1.5 °C between 2030 and 2052.[1]

Microbial fuel cell (MFC) is a new type of energy conversion device that is capable of producing clean electricity while treating wastewater streams. In MFCs, the electroactive bacteria oxidize the volatile matter in wastewater at the anode releasing electrons to the cathode through an external circuit.[2−4] At the cathode, the electrocatalyst plays a crucial role in the oxygen reduction reaction (ORR) affecting the overall power generation.[5] Platinum (Pt) and Pt-based are the most commercial electrocatalyst used for the ORR.[6] However, their limited stability, low abundance, and high cost have prevented their large-scale applications.[7] Therefore, considerable development should be taken to replace conventional Pt-based catalysts with an efficient, cost-effective catalyst to overcome the energy barriers in the redox reactions. Recently, significant research efforts have been dedicated to metal nitrogen-doped carbon matrix (M−N−C) as an electrocatalyst to replace platinum, which is simply prepared by direct carbonization of a mixture of nitrogen-rich carbon material and

Received: April 14, 2023
Accepted: October 5, 2023
Published: November 13, 2023

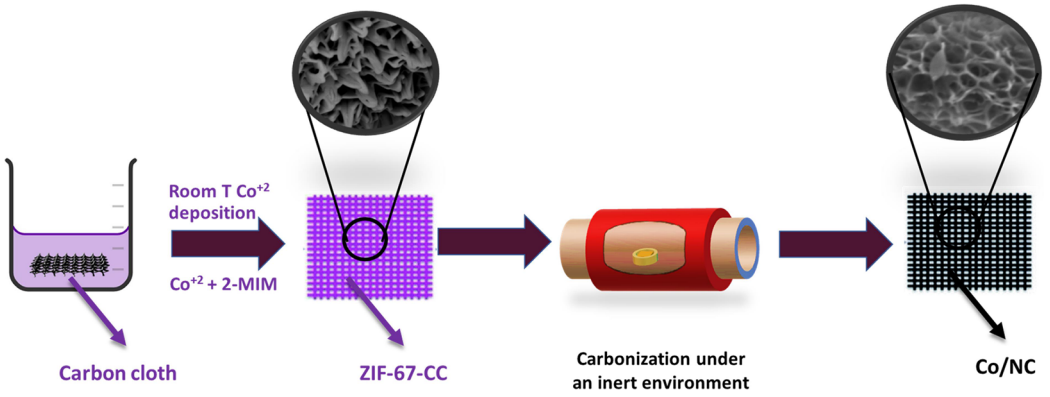

Figure 1. Schematic diagram of the fabrication of cobalt-based imidazole frameworks on carbon cloth.

transition metal.[8−13] Although the ORR activity and durability of the (M−N−C) materials are expected to be enhanced after carbonization, this might cause the catalyst to close its pores, resulting in a 2 e^- pathway. This will form H_2O_2 as an intermediate product, which could act as a poison to the catalyst.[14]

Metal−organic frameworks (MOFs) are an emerging class of compounds that offer a promising future as a candidate for ORR. Owing to their structural diversities and readily accessible active sites that can be easily tuned to make them a strong candidate to generate new active sites for redox reactions with a well-defined composition and structure.[15−19] Unfortunately, MOFs have suffered from stability issues and insufficient electronic conductivity. However, they can act as a template for ORR through a simple carbonization route while keeping their well-defined structure, size, and composition by controlling the MOF synthesis and the carbonization conditions.[20] Zeolite imidazole framework (ZIF-67) is a type of MOF that uses cobalt as the metal precursor and 2-methylimidazole (2-MIM) as the organic linker has shown excellent activity toward ORR due to the 2-MIM, which contains sufficient nitrogen compound with high tunable structure. Moreover, the substitution of cobalt has proven to show an enhancement in ORR activity.[21]

In this work, a facile and efficient approach has been developed for the synthesis of ZIF-67 as a basic support for nitrogen-doped-carbon cloth (CC@ZIF-67) as a cathode for MFCs. An in situ growth route of ZIF-67 on the carbon cloth (CC) was achieved by a simple water-based synthesis at room temperature. The study included the effect of the reaction time on the ORR followed by carbonization at different temperatures. The developed MOF-based electrodes are characterized, and their ORR activity along with their stability was investigated using three cell electrodes under alkaline conditions. With an air-cathode MFC, the developed electrode was tested and compared with state-of-the-art Pt/C and bare CC.

2. MATERIALS AND METHODS

2.1. Materials. CC was obtained from (EC-20−10, ElectroChem. Inc.). Selenium, sodium borohydride, thiourea, cobalt nitrate hexahydrate, and 2-MIM were bought from (Sigma-Aldrich, Germany). Deionized (DI) water was produced from a Milli-Q system (17 MΩ cm^{-1}). Nitric acid and sulfuric acid were obtained from Sigma-Aldrich (Germany) for the CC activation. Potassium hydroxide pellets (KOH) (Sigma-Aldrich, Germany) were used for the examination of the ORR activity. Glucose anhydrous (HiMedia, India), Phosphate buffer saline (PBS) (HiMedia, India), Peptone bacteriological (HiMedia, India), dried yeast "*Saccharomyces cerevisiae*" (*S. cerevisiae*) and yeast extract powder (HiMedia, India) were also used in this study for the MFC testing unit.

2.2. CC Treatment. A piece of CC (1 × 1 cm^2) was sonicated in ethanol solution (>97%,) for 30 min to remove organic contents and after that cleaned with distilled water. Then, the CC was preheated with concentrated H_2SO_4 and HNO_3 (molar ratio 3:1) at 60 °C for 8 h followed by several washing with di-ionized water and ethanol to neutrality.[22] Finally, the CC was dried under a vacuum (Model: VO1218A, Thermo fisher) at 90 °C for 10 h to remove impurities.

2.3. In Situ Growth of ZIF-67 on CC and Co/NC−CC Fabrication. ZIF-67 was synthesized by a simple water-based method at room temperature. In a typical process, 0.582 g of cobalt nitrite hexahydrate (Co $(NO_3)_2{\cdot}6H_2O$) was stirred using a magnetic stirrer for 30 min in 50 mL of DI water referred to as solution (A). A 1.323 g of 2-MIM was stirred in the same manner for 10 min, referred to as a solution (B). Then, solution B was quickly added to the aqueous solution (A) followed by rapid stirring at 600 rpm for 5 min before decreasing it to 200 rpm. Then, a piece of treated CC was inserted in the above solution to allow in situ growth of the imidazolate framework. After growth for 90 min at room temperature, the electrode was removed and washed several times using DI water. To remove guest molecules, the Co@MOF-CC was treated under vacuum at 90 °C for 10 h.[23] Investigating the effect of the reaction time was achieved by allowing the ZIF-67 growth on the CC at different reaction times followed by annealing for 2 h at 5 °C/min to obtain Co/NC-t (where t = 45, 90, 180, and 240 min). On the other hand, investigating the effect of annealing temperature was achieved by taking the best reaction time (e.g., 90 min) followed by annealing for 1 h at 5 °C/min under an inert environment to obtain Co/NC-T (where T = 700, 800, and 900 °C). The illustration of the fabrication process is shown in Figure 1.

2.4. MFCs Construction and Operation. Based on the best catalytically developed cathodes, a comparison with the Pt catalyst of 0.5 mg/cm^2 loading using a MFC demonstrates the feasibility of the Co/NC prepared catalyst. An air-cathode reactor was constructed from cubic polyethylene drilled into the workshop to construct a cylindrical hole of 3.5 cm diameter and 6 cm length with a total volume of 25 mL. The anolyte was inoculated with 4 mL of the cultivated bacterium and 20 (g/L)

https://doi.org/10.1021/acsomega.3c02544
ACS Omega 2023, 8, 44514−44522

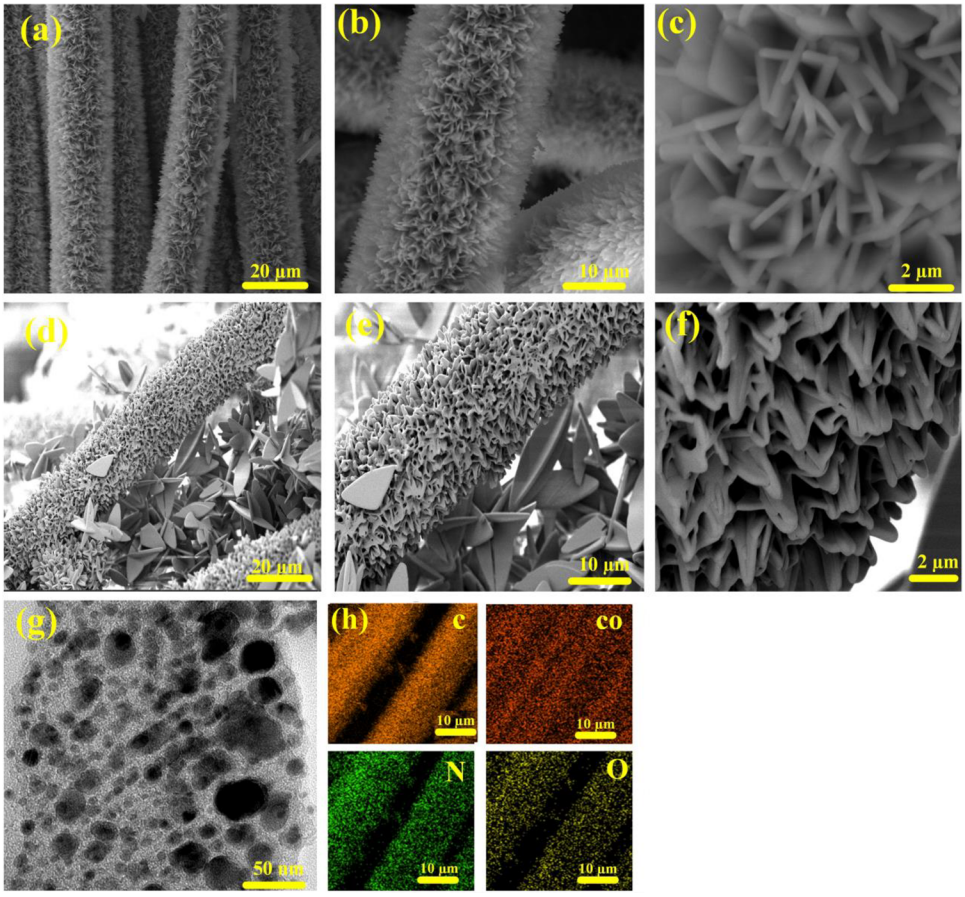

Figure 2. SEM results of Co-MOF before annealing (a) 20 μm, (b) 10 μm, and (C) 2 μm; FSEM of Co-MOF before annealing (d) 20 μm, (e) 10 μm, and (f) 2 μm; (g) TEM results of Co/NC-800 at 50 nm; and (h) elemental mapping.

glucose in a 50 mM phosphate buffer.[2] The anode was a carbon brush that was inserted in the middle of the reactor. *S. cerevisiae* was used as the electroactive bacterium to generate electrons from glucose. The membrane used was Nafion@117 (Fuel Cell Store). A titanium mesh was attached to the cathode, which served as a current collector. A rubber gasket was inserted between the blocks, which applied pressure to the membrane electrode assembly to prohibit leaks between the blocks. To ensure full anode enrichment, the MFC was kept running under open circuit voltage (OCV) for more than 1 day. After achieving a constant OCV, the power and current density calculation were started.

2.5. Electrochemical Measurements. For the evaluation of the ORR, the electrochemical measurements were performed on an SP-200 Potentiostat at room temperature (23 °C ± 2 °C) using three cell electrodes. A piece of 1 cm^2 of the developed electrode was used as the working electrode with Ag/AgCl as the reference electrode and 1 cm^2 Pt foil as the counter electrode. All of the measurements were conducted using 0.1 M KOH under N_2 and O_2. Before collecting the data, cyclic voltammetry (CV) was applied for more than 50 cycles at a scanning rate of 50 mV/s until the curves stabilized. To analyze the redox performance of the developed electrode, CV, linear sweep voltammetry (LSV), and oxygen reduction current I_{ORR} measurement was conducted in an alkaline medium (0.1 KOH) at a range of potential starting from 0.2 to −0.8 V under O_2 and N_2 at a scanning rate of 5 mV/s.

A fuel cell test was conducted on the prepared MFC at room temperature (23 ± 2 °C). The open circuit potential was recorded using a data logger "Graphtec midi LOGGER GL 240" versus Ag/AgCl reference electrode until stable potential was obtained after 18−24 h. After that, the closed test measurements were conducted on an SP-200 potentiostat at room temperature (23 °C ± 2 °C).

To measure the stability and durability of the synthesized electrode, CV analyses were conducted under O_2 for 1000 cycles (at 100 mV/s) between −0.8 and 0.2 V using three-electrode cells. The electrolyte used was 0.1 M KOH and a piece of 1 cm^2 of the developed electrode, Ag/AgCl, and a 1 cm^2 Pt electrode as working, reference, and counter electrodes, respectively.

2.6. Characterization. The surface morphology and elemental analysis of the samples were performed using scanning electron microscopy (SEM, Tescan XMU), and transmission electron microscopy (TEM, Jeol JEM-2100). The crystallinity of the prepared electrodes was determined by using powder X-ray diffraction (PXRD, TESCAN VEGA3, Bruker D8). A quick scan was performed at a range of $5° \leq 2\theta \leq 90°$ to identify the range of the peaks, and based on the quick scan the range was chosen. Fourier transform infrared-attenuated total reflection (FTIR-ATR) spectra were scanned on a Fourier transform spectrometer (Jasco, FT/IR-6800, Denmark). Spectra were acquired in the range of 400−4000 cm^{-1} with a spectral resolution of 4 cm^{-1}. The X-ray photoelectron spectroscopy (XPS) was conducted on a (Nexsa G2, Thermoscientific) spectrometer.

https://doi.org/10.1021/acsomega.3c02544
ACS Omega 2023, 8, 44514−44522

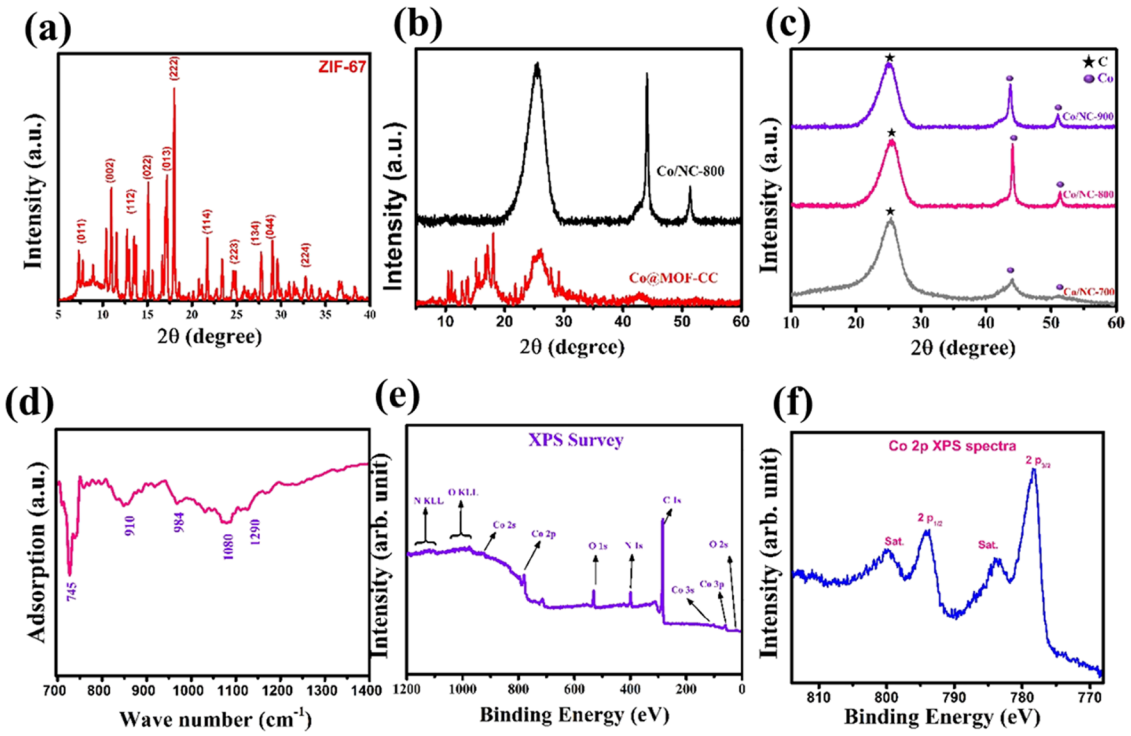

Figure 3. (a) XRD data for ZIF-67 powder; (b) XRD data for the developed electrode before annealing (Co@MOF-CC) and after annealing for 1 h at 800 °C (Co/NC-800); (c) XRD data for the developed electrode Co/NC−CC at different annealing temperature (MOF-700, MOF-800, and MOF-900); (d) FTIR spectrum of MOF-800; (e) XPS survey of Co/NC-800; and (f) Co 2p spectrum of Co/NC-800.

The specific surface areas of the MOFs were calculated by using the Brunauer−Emmett−Teller (BET) equation. BET is a standard method for determining the surface area of the obtained porous MOFs from N_2 adsorption isotherms at 77 K.[24] In this study, the surface area was determined using a BET surface area and pore size analyzer (Quanta chrome NOVA 2200e). By starting the degassing at 300 °C for 3 h followed by the sample analysis under nitrogen liquid.

3. RESULTS AND DISCUSSIONS

The growth of the zeolitic imidazole framework (ZIF-67) on the CC was observed by using SEM. As shown in Figure 2 a−c, the macroscopic structure indicates that ZIF-67 uniformly covers the CC forming a shell structure with nanowire-like morphology.[25] At higher magnification (Figure 2c), a shear plane of the nanosheet was revealed with a vertical and horizontal flake-like morphology. Such a microporous structure enhances the sluggish ORR kinetics and facilitates the electrolyte mass transport owing to their higher active sites. Furthermore, FSEM was conducted to get more obvious results for the developed electrode. Figure 2 d−f shows pronounced nanowire-like morphology with the presence of nanoflower-like crystal.

SEM images of Co@MOF-CC at different reaction times were obtained. Figure S1a,a',b,b',c,c',d,d' shows the morphological structure for MOF-A, MOF-B, MOF-C, and MOF-D, respectively, at 3 and 20 kX magnification, where *A*, *B*, *C*, and *D* represent different reaction times, namely, 45, 90, 180, and 240 min, respectively. Despite the difference in the reaction time, all the CC electrodes revealed a similar morphology of ZIF-67 covering the carbon tubes with a shell structure nanowire-like structure. However, increasing the reaction time to 180 and 240 min results in the nucleation of a new crystal structure, where a 3D hollow fiber-like flower can be noticed (Figure S1c). Furthermore, there is a clear difference between the crystal size and thickness (Figure S1a',b',c',d'), especially for Co@MOF-D (Figure S1d') where a distinct difference in the lateral size and sheet thickness can be noticed, suggesting more deposition of ZIF-67 on the CC. This could be attributed to the constant ratio of the organic linker (2-MIM), and the fact that ZIF-67 was prepared at room temperature, which may cause further linkage with the metal ion.[26,27] Interestingly, it was noticed that the developed Co/NC-800 electrode kept its identity after annealing (Figure S2) and after performing the stability test for 1000 cycles under O_2 conditions in 0.1 M KOH at a scanning rate of 50 mV/s (Figure S3).

For further exploration of the developed electrode, the Co/NC-800 nanostructure was confirmed by TEM as depicted in Figure 2g,h. The low magnification of the developed Co/NC-800 electrode reveals the distribution of the cobalt nanoparticles over the carbon surface with an average diameter of 19 nm.[28,29]

The BET tests were carried out on Co/NC-800 and plain CC (Figure S5). The surface areas calculated for the samples were found to be 161.5 $m^2\ g^{-1}$ for the developed electrode (Co/NC-800), while plain CC revealed a lower BET surface area of 10.9 $m^2\ g^{-1}$.[30] This is consistent with the SEM result between Co/NC-800 (Figure 2a) and plain CC (Figure S6) indicating the growth of ZIF-67 nanosheets have created more active sites for ORR kinetics.

The crystalline structure of the catalyst was obtained by using PXRD analysis (Figure 3a−c). The XRD spectra in Figure 3a show all of the observed peaks attributed to the ZIF-67. The notable peaks in the XRD pattern of this prepared MOF can be listed as 7.5° (011), 11.4° (002), 12.7° (112),

https://doi.org/10.1021/acsomega.3c02544
ACS Omega 2023, 8, 44514−44522

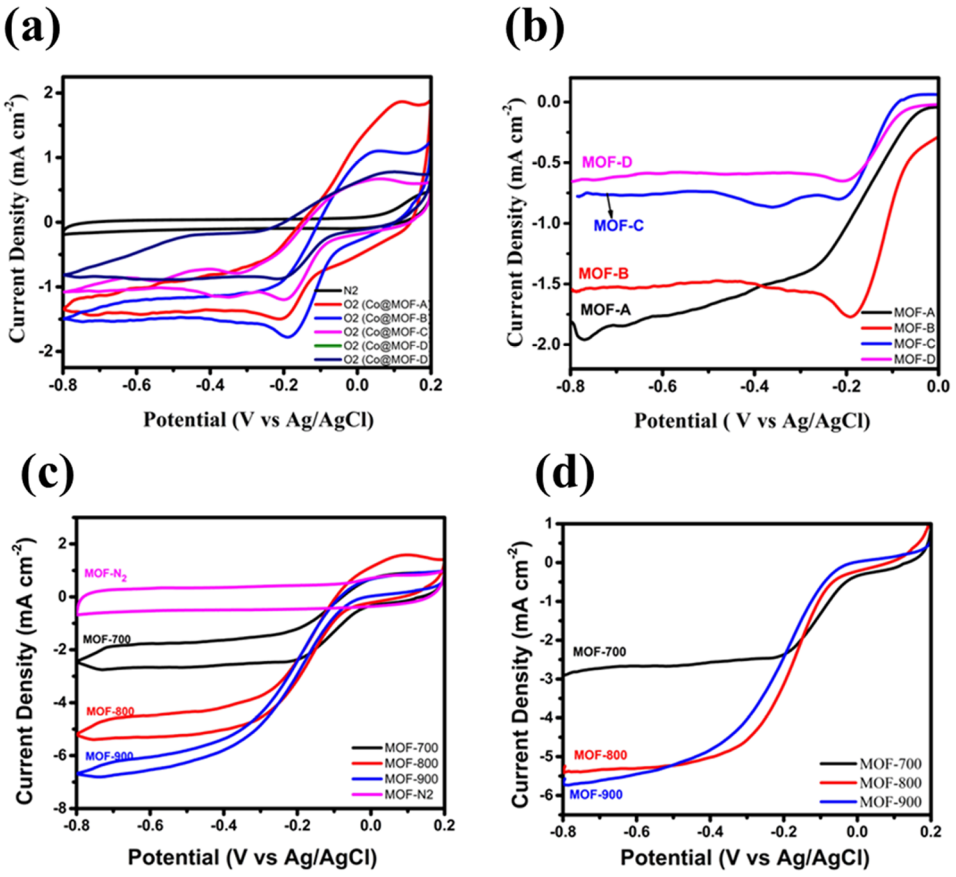

Figure 4. (a) Cyclic voltammetry of MOF-A, MOF-B, MOF-C, and MOF-D in 0.1 M KOH at a scanning rate of 5 mV/s; (b) IORR of MOF-A, MOF-B, MOF-C, and MOF-D in 0.1 M KOH at a scanning rate of 5 mV/s; (c) cyclic voltammetry of MOF-700, MOF-800, and MOF-900 in 0.1 M KOH at a scanning rate of 5 mV/s; and (d) IORR of MOF-700, MOF-800, and MOF-900 in 0.1 M KOH at a scanning rate of 5 mV/s.

15.2° (022), 17° (013), 18° (222), 21.7° (114), 24.8° (233), 25.6° (002), 27.7° (134), 29.01° (044), and 32.8° (244), suggesting the growth of the 2D crystal structure of the (ZIF-67).[31] The XRD pattern for ZIF-67 was compared with the simulated pattern (COD ref. Card:7222297), as shown in Figure S4. According to these spectra, the XRD patterns are in agreement with the simulated pattern, confirming the phase purity and crystalline structure of the synthesized sample. However, there is a small shift on the angle to the left, indicating small defects in the particle size, which could be attributed to the different preparation methods, including room temperature, rate of mixing, and most importantly the 2-MIM/Co^{2+} ratio, which play an important role during ZIF-67 crystal formation.[26,32] Figure 3b shows a comparison of the XRD peaks of the developed electrode before and after annealing for 1 h at 800 °C, Co@MOF-CC and Co/NC-800, respectively. The results indicate that all the peaks located at 2-theta, namely, 10, 15, 17, 19, 22.2, 23.9, 27.2, and 30.1 reveal the crystallinity of the ZIF-67. After pyrolysis, three noticeable peaks were observed, namely, 26.1, 43.9, and 53.4, for the carbon peak and cobalt metal, respectively, in the case of Co/NC−CC (Figure 3b). The XRD patterns for the temperature effect are displayed in Figure 3c. After annealing, three noticeable broad peaks were observed for all three electrodes, Co/NC-700, Co/NC-800, and Co/NC-900, namely, 26.1° for the carbon peak and 43.9, and 53.4° for the cobalt metal, respectively.[33] These strong diffraction peaks reveal the excellent crystallinity of Co/NC. Note that the intensity of the XRD peaks increases with increasing carbonization temperature, indicating more graphitization and crystallization of Co/NC−CC at high temperatures.

Growth of the ZIF-67 on the CC was also confirmed using the FTIR spectrum (Figure 3d). The appearance of the absorption peak at 745 cm^{-1} is attributed to the imidazole ring blending,[25] while the appearance of the peak at 994 cm^{-1} is due to the C−N stretching. Finally, the other peaks between 1000 and 1400 cm^{-1} indicate the presence of C−O and C═C functional groups.[34,35]

XPS was conducted to investigate the surface composition and chemical state of the developed catalyst. The results of the XPS survey (Figure 3e) revealed the presence of four elements including Co, C, N, and O. Notably, the presence of oxygen is mainly due to the cobalt shallow oxidation during air exposure. The results of the Co 2p spectrum (Figure 3 f) show peaks at ∼799.9 and ∼783.7 eV, which are ascribed to the satellite Co 2p, while the spectra at ∼790.3 and ∼778.2 eV are attributed to the 2 $p_{1/2}$ and 2 $p_{3/2}$, respectively.[25,36]

3.1. Electrochemical Performance of Co/NC/ZIF-67.

To evaluate the effectiveness of the developed electrode, different electrochemical measurements were performed. The most important factor affecting the activity of the catalyst in the ORR reaction is the $E_{1/2}$ potential. The $E_{1/2}$ and the onset potential can be found from the LSV under N_2 and O_2 provisions. All tests were performed on an alkaline solution (0.1 M KOH) using a standard three-electrode cell Ag/AgCl, Pt, and the developed electrode as the reference, counter, and working electrodes. To evaluate the best activity, different

https://doi.org/10.1021/acsomega.3c02544
ACS Omega 2023, 8, 44514−44522

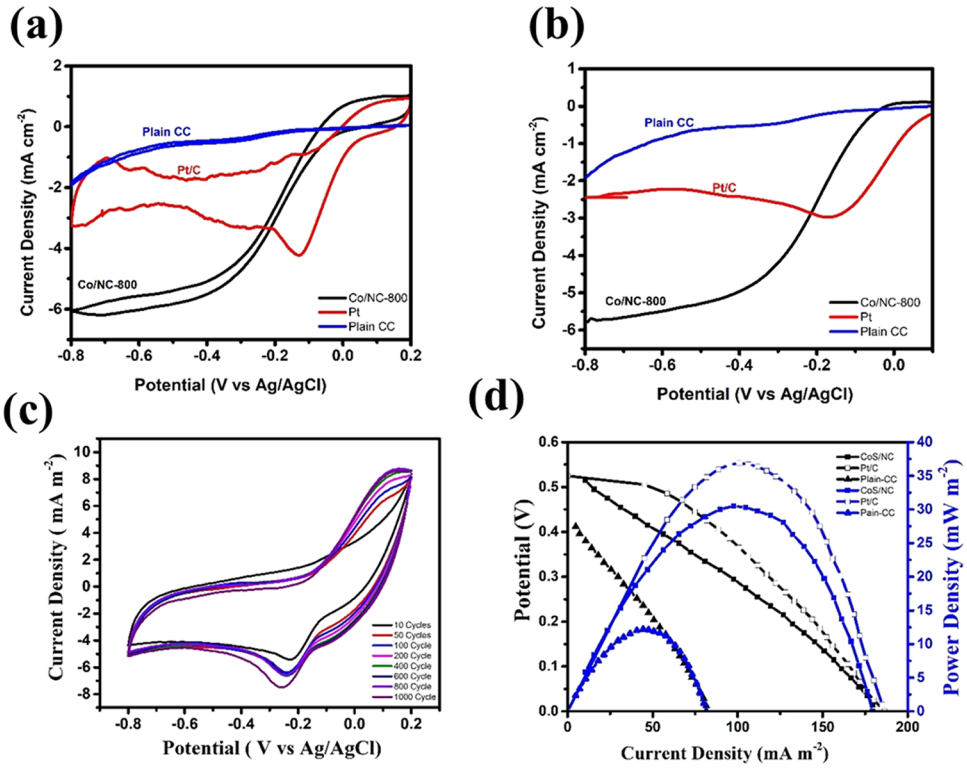

Figure 5. (a) Cyclic voltammetry of Co/NC-800, and Pt-CC in 0.1 M KOH at a scanning rate of 5 mV/s; (b) IORR for Co/NC-800, and Pt-CC in 0.1 M KOH at a scanning rate of 5 mV/s; (c) stability test of Co/NC-800 in 0.1 M KOH at a scanning rate of 50 mV/s for 1000 cycles; and (d) polarization and power density curves of plain CC, Co/NC-800, and Pt/CC.

reaction times and different annealing temperatures for the N-doped CC for better ORR performance were considered.

In order to study the effect of reaction time on the ORR performance, four electrodes were prepared using different reaction syntheses, namely, at 45 min (MOF-A), 90 min (MOF-B), 180 min (MOF-C), and 240 min (MOF-D), each followed by carbonization at a ramping rate of 5 °C/min for 2 h under vacuum before starting the electrochemical measurements. Figure 4a shows the CV of the developed electrodes under the O_2 at different reaction times and under N_2. It is seen (Figure 4 a) that there are no characteristic peaks in the cycle in the case of N_2. This demonstrates the stability of the developed catalyst (Co-MOF-t) on the pristine CC. However, in the case of O_2, the cathodic and the anodic peaks can be observed, confirming the activity of the developed catalyst. Figure 4b presents results for LSV of the developed electrode at different reaction times. A reaction time of 90 min (MOF-B) reveals the best performance on the onset potential 0 V vs Ag/AgCl, half-wave potential −0.1 V vs Ag/AgCl, and limited current −1.51 mA/cm^2 compared to 180 and 240 min with an onset potential of −0.1 V Ag/AgCl and half-wave potential of −0.16 V Ag/AgCl and a low current density of 0.74 and 0.75 mA/cm^2 for MOF-D and MOF-C, respectively (Figure 4b). Therefore, it can be concluded that increasing the reaction time beyond 90 min has a negative impact on the ORR performance. This is as evidenced by the SEM results (Figure S1), which may be attributed to the fact that the thickness of the nanosheets increases with time, affecting the active sites of the redox reaction and thus mass transfer limitations. The annealing temperature for the reaction time effect was 800 °C for 2 h. The effect of annealing time (1 and 2 h) was investigated, as shown in Figure S7. As is clear from Figure S7, the effect of annealing time has shown an effect in terms of the limiting current density at a higher potential. This could be attributed to the relation between the degree of carbon graphitization, which will affect the crystallinity and the density of the sample. Therefore, at lower annealing time, the limited current density was found to be −5.7 mA/cm^2 for 1 h compared to −1.5 mA/cm^2 for 2 h annealing.[37]

Carbonization on MOF-based materials aims to produce a porous carbon-based catalyst by keeping the template of the MOF with the metal ions, and thus better expected performance. In this study, Co@MOF-CC was carbonized at 700, 800, and 900 °C. The results are shown in Figure 4c,d at different temperatures (MOF-T) at a ramping rate of 5 °C/min for 1 h under an inert environment. Starting with the onset potential, the results demonstrate that the developed electrodes have a similar over potential at different temperatures at around 0 vs V Ag/AgCl. MOF-700 showed poor performance with a limited current density of 3 mA/cm^2. When the annealing temperature increased by 100 °C (i.e., MOF-800), the activity was noticeably improved with a limited current density of 5.4 mA/cm^2, which represents the maximum diffusion current density and a half-wave potential of −0.12 vs V Ag/AgCl. When the pyrolysis temperature was further increased to 900 °C, the overpotential was slightly increased, thus decreasing the ORR performance in terms of the onset potential; however, it showed a higher limited current density of 5.6 mA/cm^2. This higher limited current density indicates a higher mass diffusion of the oxygen to the active sites. Such performance could be related to the effect of the temperature on increasing the graphitization of the samples, by using a higher temperature, more amorphous content will be eliminated (may also increase the porosity); however, at the

https://doi.org/10.1021/acsomega.3c02544
ACS Omega 2023, 8, 44514−44522

same time increasing the temperature would result in decreasing the nitrogen content that plays important role in the ORR activity.[38] To summarize, an annealing temperature of 800 °C revealed the best ORR activity. This could be attributed again to the balance between the degree of graphitization (affects electrical conductivity) and the nitrogen content (affects the number of the ORR active sites).

Comparing the developed electrode with the commercialized state-of-the-art Pt/C one, the developed catalyst (Co/NC-800) showed an enhancement in the limited current density with around 0.8 mA/cm^2, which is almost 2.2 times higher than that of commercial Pt/C (Figure 5 a,b). In terms of the onset potential, the Pt/C showed a lower overpotential than the Co/NC-800 with around 120 mV. For comparison with plain CC, the CV analysis of plain CC (untreated CC) was also measured where it showed a very low catalytic activity (Figure 5a,b). The stability test of Co/NC-800 was conducted by measuring CV for 1000 cycles under the O_2 conditions in 0.1 M KOH at a scanning rate of 50 mV/s. The developed electrode demonstrated higher stability at this scan rate (Figure 5 c). A well-developed cathodic and anodic peak can be also observed (Figure 5 c), and they are almost constant after 50 cycles.

3.2. MFC Using Co/NC-800 and Pt/C Electrodes. The previous analysis was based on an ex situ measurement of the developed electrode performance. In this section, an air-cathode MFC was used as an in situ performance assessment for the developed electrode. Three small MFCs were prepared using a carbon brush as the anode for all tested MFCs, while the cathode was plain CC, Pt/CC. The Co/NC-800 was used to perform an in situ comparison of the developed electrode with the commercial state-of-art platinum and with plain CC.

The cell was operated to achieve a constant open circuit. The cells were then taken for analysis using a potentiostat with variable resistance to construct the polarization and power density curves. The polarization and power density curves are displayed in Figure 5d for the **plain CC, Co/NC-800, and Pt/CC**). According to Figure 5d, the three MFCs reveal almost a similar trend of the losses observed, which is attributed to the fact that all the parameters were the same for the three MFCs and the only difference was the cathode, which clearly explains the observed difference in the potential. The potential of the plain CC started at 0.41 V, which is lower than that of the Co/NC-800 and Pt/C with 130 mV. Plain CC achieved power and current densities of 12 ± 2.5 mW/m^2 and 81 ± 2.5 mA/m^2, respectively, which is lower 2.5-fold than the developed electrode in this work (Co/NC-800). Comparing the developed electrode with the commercial platinum CC, CoS/NC achieved a maximum power density of 30 ± 2.5 mW/m^2 and a maximum current density of 180 ± 2.5 mA/m^2, which is almost comparable to Pt/C with maximum current and power densities of 36 ± 2.5 mW/m^2 and 186 ± 2.5 mA/m^2, respectively. To sum up, the ORR enhancement was related to the effect of cobalt metal, nitrogen doping, and MOF effect to create new active sites for ORR.[39,40]

4. CONCLUSIONS

A novel electrode for a MFC was developed using a MOF as a template for CC to enhance the porosity and the conductivity for the ORR in MFC. The developed electrode (Co/NC) revealed a uniform nanowire-like morphology that encapsulated the nanorods of the CC. The developed catalyst (Co/NC-800) was able to enhance the ORR activity with promising results that are comparable to commercialized state-of-the-art Pt/C. Comparing the developed electrode in this work with Pt/C, platinum-based showed a more positive onset potential with only 120 mV. The developed electrode (Co/NC-800) also revealed a higher limited current density compared to Pt/C. An enhancement in the bioelectricity generated by using the developed electrode in this work (Co/NC-800) by 3.5-fold compared to plain CC was achieved upon implementation of MFC. Comparing the developed electrode (Co/NC-800) with the commercial Pt/C showed that the developed electrode (Co/NC-800) was capable of generating power close to that of the Pt/C, which proves the enhancement of the ORR kinetic on a real MFC. This demonstrates that Co@ZIF-67 has remarkable electrocatalytic activity in fuel cell applications.

■ ASSOCIATED CONTENT

Supporting Information

The Supporting Information is available free of charge at https://pubs.acs.org/doi/10.1021/acsomega.3c02544.

SEM results for the effect of the reaction time on Co@MOF; morphological structure of the Co/NC@CC after carbonization and after stability test for 1000 cycle; average diameter of Co particles from TEM at 50 nm; XRD of ZIF-67; adsorption−desorption isotherms of Co/NC-800 and plain CC; SEM of plain carbon cloth; and effect of annealing time at 800 °C for Co/NC (PDF)

■ AUTHOR INFORMATION

Corresponding Author

Sameer Al-Asheh − *Department of Chemical Engineering, American University of Sharjah, Sharjah 26666, United Arab Emirates;* orcid.org/0000-0003-1012-427X; Email: sslasheh@aus.edu

Authors

Mohammed Al Murisi − *Department of Chemical Engineering, American University of Sharjah, Sharjah 26666, United Arab Emirates*

Mohammad Ali Abdelkareem − *Department of Sustainable and Renewable Energy Engineering, University of Sharjah, Sharjah 27272, United Arab Emirates*

Ahmad Aidan − *Department of Chemical Engineering, American University of Sharjah, Sharjah 26666, United Arab Emirates*

Khaled Elsaid − *Chemical Engineering Program, Texas A&M University at Qatar, Doha 23874, Qatar*

Abdul Ghani Olabi − *Department of Sustainable and Renewable Energy Engineering, University of Sharjah, Sharjah 27272, United Arab Emirates*

Complete contact information is available at: https://pubs.acs.org/10.1021/acsomega.3c02544

Notes

The authors declare the following competing financial interest(s): The authors declare they have no known competing financial interests or personal relationships that could have appeared to influence the work reported in this paper.

https://doi.org/10.1021/acsomega.3c02544
ACS Omega 2023, 8, 44514−44522

■ ACKNOWLEDGMENTS

The authors acknowledge the support provided by the Open Access Program from the American University of Sharjah. Special thanks to the Department of Sustainable and Renewable Energy Engineering for providing access to different equipment's used for the characterization of the developed electrodes.

■ REFERENCES

(1) Masson-Delmotte, V.; Zhai, P.; Pörtner, H.; Roberts, D.; Pirani, A. Global warming of 1.5°C, *Intergovernmental Panel on Climate Change* 2019. Accessed: Jun. 18, 2023. [Online]. Available: https://www.ipcc.ch/site/assets/uploads/sites/2/2019/06/SR15_Full_Report_Low_Res.pdf.

(2) Sayed, E. T.; Abdelkareem, M. A.; Alawadhi, H.; Elsaid, K.; Wilberforce, T.; Olabi, A. G. Graphitic carbon nitride/carbon brush composite as a novel anode for yeast-based microbial fuel cells. *Energy* **2021**, *221*, No. 119849.

(3) Ramya, M.; Senthil Kumar, P. A review on recent advancements in bioenergy production using microbial fuel cells. *Chemosphere* **2022**, *288*, No. 132512.

(4) Al-Murisi, M.; Al-Muqbel, D.; Al-Othman, A.; Tawalbeh, M. Integrated microbial desalination cell and microbial electrolysis cell for wastewater treatment, bioelectricity generation, and biofuel production: Success, experience, challenges, and future prospects, in *Integrated Environmental Technologies for Wastewater Treatment and Sustainable Development*; Elsevier 2022, 145−166.

(5) Das, I.; Noori, M. T.; Shaikh, M.; Ghangrekar, M. M.; Ananthakrishnan, R. Synthesis and Application of Zirconium Metal−Organic Framework in Microbial Fuel Cells as a Cost-Effective Oxygen Reduction Catalyst with Competitive Performance. *ACS Appl. Energy Mater.* **2020**, *3* (3), 3512−3520.

(6) Cruz-Martínez, H.; Rojas-Chávez, H.; Matadamas-Ortiz, P. T.; Ortiz-Herrera, J. C.; López-Chávez, E.; Solorza-Feria, O.; Medina, D. I. Current progress of Pt-based ORR electrocatalysts for PEMFCs: An integrated view combining theory and experiment. *Mater. Today Phys.* **2021**, *19*, No. 100406.

(7) Yan, Y.; Hou, Y.; Yu, Z.; Tu, L.; Qin, S.; Yuan, G.; Lan, D.; Chen, S.; Sun, J.; Wang, S. Bimetallic organic framework-derived, oxygen-defect-rich FexCo3-xS4/FeyCo9-yS8 heterostructure microsphere as a highly efficient and robust cathodic catalyst in the microbial fuel cell. *J. Power Sources* **2020**, *472*, No. 228582.

(8) Wu, Z.-S.; Chen, L.; Liu, J.; Parvez, K.; Liang, H.; Shu, J.; Sachdev, J.; Graf, R.; Feng, X.; Müllen, K. High-performance electrocatalysts for oxygen reduction derived from cobalt porphyrin-based conjugated mesoporous polymers. *Adv. Mater.* **2014**, *26*, 1450−1455.

(9) Xia, W.; Mahmood, A.; Liang, Z.; Zou, R.; Guo, S. Earth-abundant nanomaterials for oxygen reduction. *Angew. Chem., Int. Ed.* **2016**, *55*, 2650−2676.

(10) Quílez-Bermejo, J.; Morallón, E.; Cazorla-Amorós, D. Metal-free heteroatom-doped carbon-based catalysts for ORR: A critical assessment about the role of heteroatoms. *Carbon* **2020**, *165*, 434−454.

(11) Gong, K.; Du, F.; Xia, Z.; Durstock, M.; Dai, L. Nitrogen-doped carbon nanotube arrays with high electrocatalytic activity for oxygen reduction. *Science* **2009**, *323*, 760−764.

(12) Zhu, J.; Huang, Y.; Mei, W.; Zhao, C.; Zhang, C.; Zhang, J.; Amiinu, I.; Mu, S. Effects of Intrinsic pentagon defects on electrochemical reactivity of carbon nanomaterials. *Angew. Chem., Int. Ed.* **2019**, *58*, 3859−3864.

(13) Wang, Z.; Jin, H.; Meng, T.; Liao, K.; Meng, W.; Yang, J.; He, D.; Xiong, Y.; Mu, S. Fe, Cu-coordinated ZIF-derived carbon framework for efficient oxygen reduction reaction and zinc-air batteries. *Adv. Funct. Mater.* **2018**, *28*, No. 1802596.

(14) Wang, C.; Li, Z.; Wang, L.; Niu, X.; Zhang, S.; Liu, Y. 3D GBM-supported transition metal oxide nanocatalysts and heteroatom-doped 3D graphene electrocatalysts for potential application in fuel cells, 2021, 139−178. DOI: 10.1039/9781839162480-00139.

(15) Shang, H.; Jiang, Z.; Zhou, D.; Pei, J.; Wang, Y.; Dong, J.; Zheng, X.; Zhang, J. Engineering a metal−organic framework derived Mn−N 4 − C x S y atomic interface for highly efficient oxygen reduction reaction. *Chem. Sci.* **2020**, *11*, 5994−5999.

(16) Agarwal, S.; Yu, X.; Manthiram, A. A pair of metal organic framework (MOF)-derived oxygen reduction reaction (ORR) and oxygen evolution reaction (OER) catalysts for zinc-air batteries. *Mater. Today Energy* **2020**, *16*, No. 100405.

(17) Li, J.; Li, G.; Wang, J.; Xue, C.; Li, X.; Wang, S.; Han, B.; Yanga, M.; Li, L. A novel core−double shell heterostructure derived from a metal−organic framework for efficient HER, OER and ORR electrocatalysis. *Inorg. Chem. Front.* **2020**, *7*, 191−197.

(18) Al Obeidli, A.; Ben Salah, H.; Al Murisi, M.; Sabouni, R. Recent advancements in MOFs synthesis and their green applications. *Int. J. Hydrogen Energy* **2022**, *47*, 2561−2593.

(19) Al-Othman, A.; Tawalbeh, M.; Temsah, O.; Al-Murisi, M. Industrial challenges of MOFs in energy applications; In *Reference Module in Materials Science and Materials Engineering*; Elsevier 2020.

(20) Lu, X. F.; Xia, B. Y.; Zang, S.; Lou, X. W. Metal−organic frameworks based electrocatalysts for the oxygen reduction reaction. *Angew. Chem., Int. Ed.* **2020**, *59*, 4634−4650.

(21) Wang, X.; Li, Z.; Qu, Y.; Yuan, T.; Wang, W.; Wu, Y.; Li, Y. Review of metal catalysts for oxygen reduction reaction: From nanoscale engineering to atomic design. *Chem.* **2019**, *5*, 1486−1511.

(22) Xu, Z.; Wang, Q.; Zhangsun, H.; Zhao, S.; Zhao, Y.; Wang, L. Carbon cloth-supported nanorod-like conductive Ni/Co bimetal MOF: A stable and high-performance enzyme-free electrochemical sensor for determination of glucose in serum and beverage. *Food Chem.* **2021**, *349*, No. 129202.

(23) Mondloch, J. E.; Karagiaridi, O.; Farha, O. K.; Hupp, J. T. Activation of metal−organic framework materials. *CrystEngComm* **2013**, *15*, 9258.

(24) Walton, K. S.; Snurr, R. Q. Applicability of the BET method for determining surface areas of microporous metal−organic frameworks. *J. Am. Chem. Soc.* **2007**, *129*, 8552−8556.

(25) Ma, J.; Li, J.; Guo, R.; Xu, H.; Shi, F.; Dang, L.; Liu, Z.; Sun, J.; Lei, Z. Direct growth of flake-like metal-organic framework on textile carbon cloth as high-performance supercapacitor electrode. *J. Power Sources* **2019**, *428*, 124−130.

(26) Guo, X.; Xing, T.; Lou, Y.; Chen, J. Controlling ZIF-67 crystals formation through various cobalt sources in aqueous solution. *J. Solid State Chem.* **2016**, *235*, 107−112.

(27) Pan, Y.; Liu, Y.; Zeng, G.; Zhao, L.; Lai, Z. Rapid synthesis of zeolitic imidazolate framework-8 (ZIF-8) nanocrystals in an aqueous system. *Chem. Commun.* **2011**, *47*, 2071.

(28) Jia, Q.; Gao, Y.; Li, Y.; Fan, X.; Zhang, F.; Zhang, G.; Peng, W.; Wang, S. Cobalt nanoparticles embedded in N-doped carbon on carbon cloth as free-standing electrodes for electrochemically-assisted catalytic oxidation of phenol and overall water splitting. *Carbon* **2019**, *155*, 287−297.

(29) Jiang, G.; Jiang, N.; Zheng, N.; Chen, X.; Mao, J.; Ding, G.; Li, Y.; Sun, F.; Li, Y. MOF-derived porous Co3O4-NC nanoflake arrays on carbon fiber cloth as stable hosts for dendrite-free Li metal anodes. *Energy Storage Mater.* **2019**, *23*, 181−189.

(30) Singh, A. K.; Yasri, N.; Karan, K.; Roberts, E. P. L. Electrocatalytic activity of functionalized carbon paper electrodes and their correlation to the fermi level derived from raman spectra. *ACS Appl. Energy Mater.* **2019**, *2*, 2324−2336.

(31) Guan, C.; Zhao, W.; Hu, Y.; Lai, Z.; Li, X.; Sun, S.; Zhang, H.; Cheetham, A. K.; Wang, J. Cobalt oxide and N-doped carbon nanosheets derived from a single two-dimensional metal−organic framework precursor and their application in flexible asymmetric supercapacitors. *Nanoscale Horiz.* **2017**, *2*, 99−105.

(32) Li, X.; Tang, B.; Huang, W.; Yu, H. Effect from mechanical stirring time and speed on adsorption performance of ZIF-90 for n-hexane. *Z. Anorg. Allg. Chem.* **2019**, *645*, 73−78.

https://doi.org/10.1021/acsomega.3c02544
ACS Omega 2023, 8, 44514−44522

(33) Yang, L.; Ding, H.; Xu, G.; Zhang, L.; Wei, B. Efficient ORR activity of N-doped porous carbon encapsulated cobalt electrocatalyst derived from a novel bimetal-organic framework. *Mater. Res. Bull.* **2021**, *138*, No. 111237.
(34) Sundriyal, S.; Shrivastav, V.; Kaur, H.; Mishra, S.; Deep, A. High-performance symmetrical supercapacitor with a combination of a ZIF-67/rGO composite electrode and a redox additive electrolyte. *ACS Omega* **2018**, *3*, 17348−17358.
(35) Parkash, A. CTAB-caped Cu nanoparticles doped on zeolitic imidazolate framework-ZIF-67 as bifunctional catalysts for oxygen-reduction and evolution reactions in alkaline media. *J. Porous Mater.* **2021**, *28*, 1245−1260.
(36) Chen, T.-Y.; Kuo, T.-R.; Yougbaré, S.; Lin, L.-Y.; Xiao, C.-Y. Novel direct growth of ZIF-67 derived Co3O4 and N-doped carbon composites on carbon cloth as supercapacitor electrodes. *J. Colloid Interface Sci.* **2022**, *608*, 493−503.
(37) Katirci, R.; Walls, J. M. The effect of annealing pressure and time on the crystallinity of CZTSe. *Surf. Rev. Lett.* **2019**, *26*, 1850151.
(38) Abdelkareem, M. A.; Wilberforce, T.; Elsaid, K.; Sayed, E. T.; Abdelghani, E. A. M.; Olabi, A. G. Transition metal carbides and nitrides as oxygen reduction reaction catalyst or catalyst support in proton exchange membrane fuel cells (PEMFCs). *Int. J. Hydrogen Energy* **2021**, *46*, 23529−23547.
(39) Skorupska, M.; Ilnicka, A.; Lukaszewicz, J. P. The effect of nitrogen species on the catalytic properties of N-doped graphene. *Sci. Rep.* **2021**, *11*, 23970.
(40) Zitolo, A.; Ranjbar-Sahraie, N.; Mineva, T.; Li, J.; Jia, Q.; Stamatin, S.; Harrington, G. F.; Lyth, S. M.; Krtil, P.; Mukerjee, S.; Fonda, E.; Jaouen, F. Identification of catalytic sites in cobalt-nitrogen-carbon materials for the oxygen reduction reaction. *Nat. Commun.* **2017**, *8*, 957.

https://doi.org/10.1021/acsomega.3c02544
ACS Omega 2023, 8, 44514−44522